Article

Cell Metabolism

PDK1-Dependent Metabolic Reprogramming Dictates Metastatic Potential in Breast Cancer

Graphical Abstract

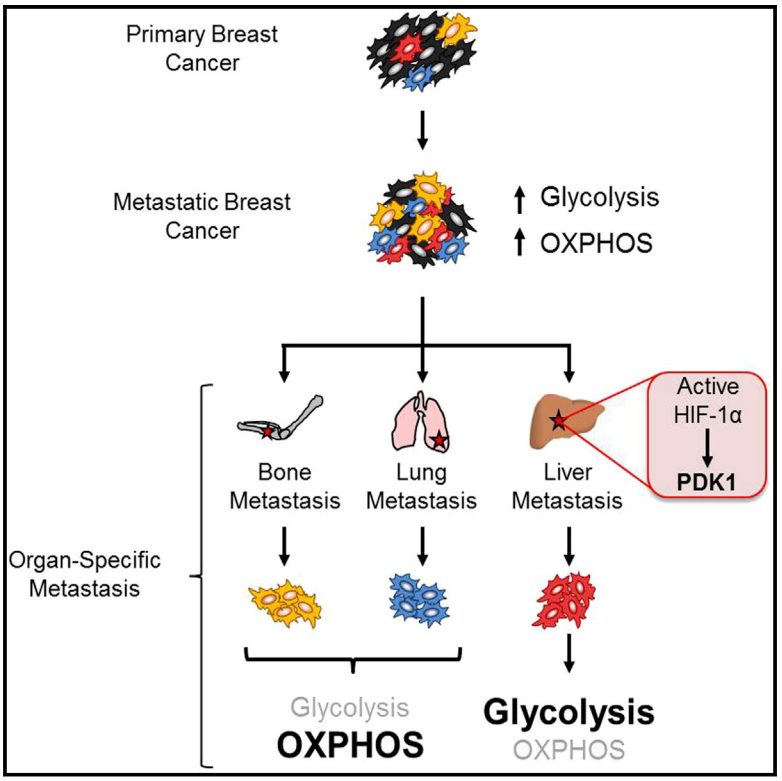

Highlights

- Breast cancer cells display unique metabolic signatures depending on metastatic site
- HIF-1α/PDK1 promotes glycolytic metabolism in liver-metastatic breast cancer cells
- PDK1 is required for efficient formation of liver metastases
- PDK1 expression is elevated in human liver metastases

Authors

Fanny Dupuy, Sébastien Tabariès, Sylvia Andrzejewski, ..., Julie St.-Pierre, Russell G. Jones, Peter M. Siegel

Correspondence

russell.jones@mcgill.ca (R.G.J.), peter.siegel@mcgill.ca (P.M.S.)

In Brief

Dupuy et al. reveal that primary breast cancer cells display extensive metabolic heterogeneity and differentially engage glycolysis or OXPHOS depending on their site of metastasis (liver, lung, or bone). Liver metastases rely on a HIF-1α/PDK1-dependent axis for their intrinsic metabolic reprogramming, which enables their efficient colonization and growth in the liver.

Dupuy et al., 2015, Cell Metabolism 22, 577–589
October 6, 2015
http://dx.doi.org/10.1016/j.cmet.2015.08.007

Cell Metabolism
Article

PDK1-Dependent Metabolic Reprogramming Dictates Metastatic Potential in Breast Cancer

Fanny Dupuy,[1,2] Sébastien Tabariès,[1,3] Sylvia Andrzejewski,[1,2] Zhifeng Dong,[1,3] Julianna Blagih,[1,4] Matthew G. Annis,[1,3] Atilla Omeroglu,[5] Dongxia Gao,[6] Samuel Leung,[6] Eitan Amir,[7] Mark Clemons,[8] Adriana Aguilar-Mahecha,[9] Mark Basik,[9] Emma E. Vincent,[1,4] Julie St.-Pierre,[1,2] Russell G. Jones,[1,4,*] and Peter M. Siegel[1,2,3,*]
[1]Goodman Cancer Research Centre
[2]Department of Biochemistry
[3]Department of Medicine
[4]Department of Physiology
McGill University, Montréal, QC H3A 1A3, Canada
[5]Department of Pathology, McGill University Health Center, Montréal, QC H4A 3J1, Canada
[6]Genetic Pathology Evaluation Centre, Department of Pathology and Laboratory Medicine, University of British Columbia, Vancouver, BC V6H 3Z6, Canada
[7]Department of Medicine, University of Toronto, Toronto, ON M5G 2M9, Canada
[8]Division of Medical Oncology, The Ottawa Hospital Cancer Centre, Ottawa, ON K1H 8L6, Canada
[9]Segal Cancer Centre, Sir Mortimer B. Davis Jewish General Hospital, Montréal, QC H3T 1E2, Canada
*Correspondence: russell.jones@mcgill.ca (R.G.J.), peter.siegel@mcgill.ca (P.M.S.)
http://dx.doi.org/10.1016/j.cmet.2015.08.007

SUMMARY

Metabolic reprogramming is a hallmark of cellular transformation, yet little is known about metabolic changes that accompany tumor metastasis. Here we show that primary breast cancer cells display extensive metabolic heterogeneity and engage distinct metabolic programs depending on their site of metastasis. Liver-metastatic breast cancer cells exhibit a unique metabolic program compared to bone- or lung-metastatic cells, characterized by increased conversion of glucose-derived pyruvate into lactate and a concomitant reduction in mitochondrial metabolism. Liver-metastatic cells displayed increased HIF-1α activity and expression of the HIF-1α target Pyruvate dehydrogenase kinase-1 (PDK1). Silencing HIF-1α reversed the glycolytic phenotype of liver-metastatic cells, while PDK1 was specifically required for metabolic adaptation to nutrient limitation and hypoxia. Finally, we demonstrate that PDK1 is required for efficient liver metastasis, and its expression is elevated in liver metastases from breast cancer patients. Our data implicate PDK1 as a key regulator of metabolism and metastatic potential in breast cancer.

INTRODUCTION

The emergence of metastatic breast cancer is the most deadly aspect of the disease, as it is largely incurable once tumor cells have spread from the primary site. Breast cancer metastasis is a complex multistep process, in which each step represents a significant barrier to metastatic progression, the most formidable being the foreign microenvironment to which disseminated cancer cells must adapt. How tumor cells overcome these barriers during metastasis is critical for successful dissemination and yet remains a poorly understood process.

One of the fundamental hallmarks of cancer is the reprogramming of cellular metabolism to promote tumor cell growth, proliferation, and survival (Hanahan and Weinberg, 2011). One of the primary metabolic changes associated with cellular transformation is increased aerobic glycolysis, also known as the "Warburg effect" (Vander Heiden et al., 2009; Warburg, 1956); however, recent work has established equally important roles for mitochondrial metabolism—the TCA cycle and oxidative phosphorylation (OXPHOS)—in tumor progression (Ahn and Metallo, 2015). Interactions between cancer cells and non-transformed cells within the tumor microenvironment, such as cancer-associated fibroblasts, may also create codependencies that help fuel the metabolic requirements of rapidly proliferating tumor cells (Chiavarina et al., 2011; Martinez-Outschoorn et al., 2014).

While considerable advances have been made in understanding how metabolic changes fuel the growth of primary tumor cells, the influence of metabolic reprogramming on the metastatic process is poorly understood. In the current study, we sought to characterize the intrinsic metabolic profiles of breast cancer cells as they spread to different metastatic sites commonly observed in human breast cancer (i.e., bone, lung, and liver). Our results indicate that while aggressively metastatic breast cancer cells displayed elevated glycolysis and OXPHOS relative to non-metastatic tumor cells, the metabolic profiles of breast cancer cells differed based on their site of metastasis. Here we have investigated the role of the Hypoxia-inducible factor-1α (HIF-1α), and its downstream target PDK1, in the regulation of metabolic reprogramming and metastatic potential in liver-metastatic breast cancer cells. Together, our data suggest that there is metabolic heterogeneity in metastatic breast cancer, and that these metabolic programs may dictate successful colonization and metastatic tumor growth at distinct sites.

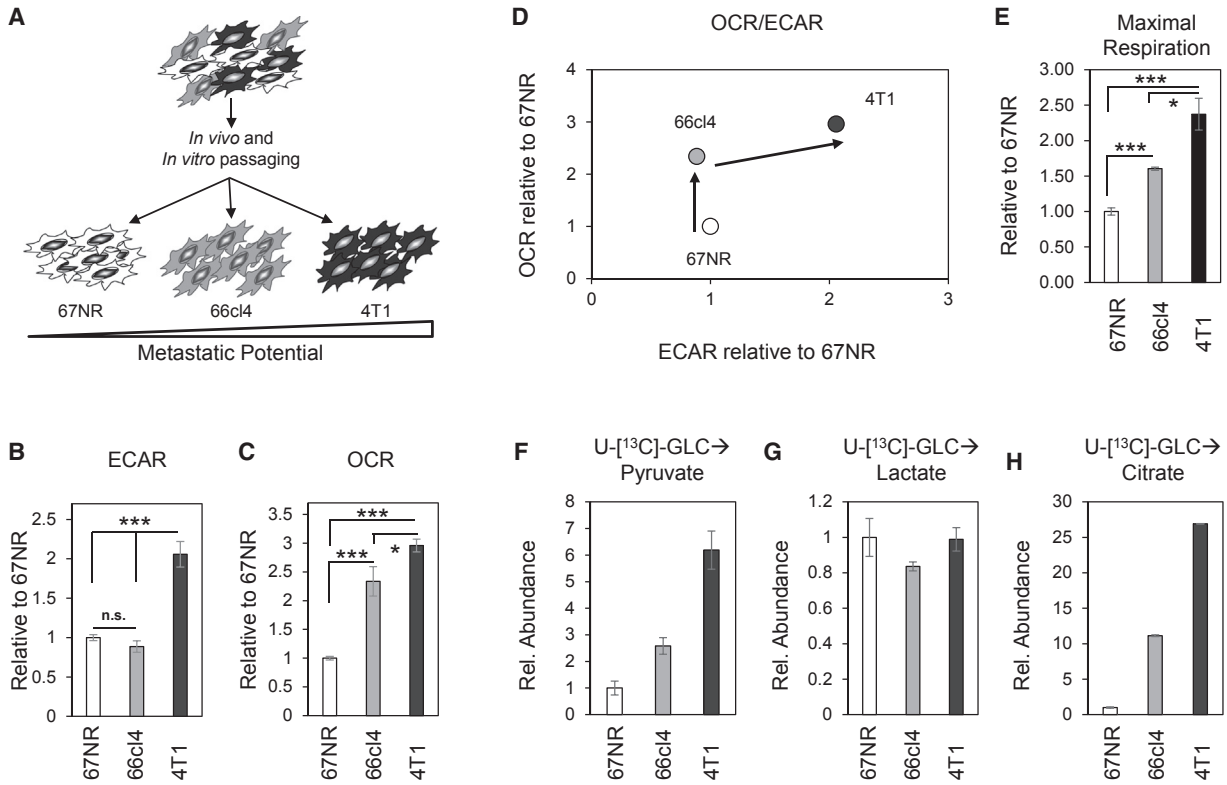

Figure 1. Increased Metabolic Activity Accompanies Enhanced Metastatic Potential

(A) Schematic of murine breast cancer cells and their associated metastatic phenotypes.

(B and C) ECAR (B) and OCR (C) are expressed as a fold change relative to 67NR.

(D) Plot representing the ratio of OCR/ECAR for each breast cancer population.

(E) Breast cancer cells were assayed for their maximal respiration measured following addition of FCCP (1.5 μM) (n = 3).

(F–H) Cells were pulsed with U-[^{13}C]-glucose for 30 min, and [^{13}C] incorporation into pyruvate (F), lactate (G), and citrate (H) was determined by GC-MS. Data represent abundance of the labeled portion of the indicated metabolite relative to 67NR for one representative experiment performed in duplicate. (B) ***$p < 0.001$ (SD); (C) ***$p < 0.001$ (SD); *$p < 0.05$ (SD); (E) ***$p < 0.001$ (SD); *$p < 0.05$. (SD).

RESULTS

Metastatic Breast Cancer Cells Display Increases in Both Glycolytic and Oxidative Metabolism

To assess metabolic differences in cancer cells exhibiting different tumorigenic and metastatic phenotypes, we used three murine breast cancer cell populations: 67NR cells that are non-metastatic, 66cl4 cells that metastasize to the lungs, and 4T1 cells that spread to various sites, including lymph nodes, bone, lung, and liver (Aslakson and Miller, 1992) (Figure 1A). We conducted bioenergetic profiling of these cells using the Seahorse XF-Bioanalyzer platform. Previous reports have shown that metastatic cancer cells possess higher levels of both glycolytic and TCA-derived metabolic intermediates relative to non-metastatic cells (Lu et al., 2010). Consistent with these results, metastatic 4T1 cells displayed an ~2-fold increase in their extracellular acidification rate (ECAR; Figure 1B), as well as increased glucose consumption and lactate production (see Figures S1A and S1B available online), relative to non-metastatic 67NR cells. Moreover, both metastatic breast cancer cell populations (66cl4 and 4T1) displayed a higher oxygen consumption rate (OCR) relative to 67NR cells (Figure 1C). This corresponded to increased OCR/ECAR ratios that were related to the metastatic potential of the breast cancer cells (Figure 1D), with 4T1 cells exhibiting significant increases in both OCR and ECAR while 66cl4 exhibited increases only in OCR. Metastatic cell populations (66cl4 and 4T1) also displayed a higher maximal respiration rate relative to 67NR cells (Figure 1E), suggesting greater oxidative capacity relative to non-metastatic breast cancer cells isolated from the same parental tumor. We further determined that these metabolic differences were not a direct consequence of increased proliferation rates, which were similar between all cell populations (Figure S1C).

We next performed stable isotope tracer analysis (SITA) using U-[^{13}C]-glucose to assess how metastatic breast cancer cells utilize glucose. Cells were pulsed with U-[^{13}C]-glucose for 30 min and the abundance of [^{13}C]-derived metabolites measured by GC-MS (schematic in Figure S1D). We observed an increase in the total abundance of [^{13}C]-glucose-derived pyruvate in cells with increasing metastatic potential: 66cl4 and 4T1 cells exhibited 2.5-fold and 6-fold increases in the total amount of [^{13}C]-glucose-derived pyruvate, respectively, relative to 67NR cells (Figure 1F). The amount of intracellular pyruvate was not dramatically different between cell

populations; however, the percentage of the pyruvate pool labeled from [^{13}C]-glucose was significantly increased in both 66cl4 and 4T1 cells relative to 67NR cells (Figure S1E), the majority of which was labeled as the m+3 isotopomer (Figure S1F).

Pyruvate can be converted into lactate to regenerate NAD, which is a hallmark of the Warburg effect. Alternatively, it can be converted to acetyl-CoA and further metabolized in the TCA cycle. Despite an increase in the glucose-derived pyruvate pool in the metastatic cells, we did not observe increased conversion of glucose-derived pyruvate to intracellular lactate (Figures 1G, S1G, and S1H). Rather, total pools and [^{13}C]-glucose-derived citrate followed the same trends as [^{13}C]-glucose-derived pyruvate (Figure 1F), which were increased in metastatic breast cancer cells (Figures 1H and S1I), with the predominant form being the m+2 isotopomer (Figure S1J).

The increased ECAR measurements observed in 4T1 cells (Figure 1B) suggest that they should be producing more lactate; however, levels of intracellular glucose-derived lactate were similar between all cell lines (Figure 1G). To confirm that 4T1 cells were indeed directing a larger portion of glucose into lactate, SITA was performed using conditioned media harvested from 67NR, 66cl4, and 4T1 cells. In agreement with our previous findings, 4T1 cells exhibit elevated levels of total pool and [^{13}C]-labeled extracellular lactate compared to 67NR and 66cl4 cells (Figure S1K), with the majority of the label found as the m+3 isotopomer (Figure S1L). Thus, unlike the conventional Warburg phenotype of primary tumor cells, highly metastatic breast cancer cells engage both glycolytic and oxidative metabolism. More importantly, these results reveal that metastatic breast cancer cells with varying degrees of metastatic fitness can differentially engage one (66cl4; OXPHOS) or multiple (4T1; glycolytic and OXPHOS) metabolic strategies.

Organ-Selective Metastatic Breast Cancer Cells Display Distinct Metabolic Programs

We next assessed whether metastatic breast cancer cells retain their metabolic phenotype following colonization of distinct metastatic sites. We previously subjected parental 4T1 cells to an in vivo selection protocol to derive subpopulations with increased selectivity for colonization and growth in specific organs. We established multiple cell populations per site—the bone (592 and 593), the lung (533 and 537), and the liver (2776 and 2792)—and confirmed that, although they retain the potential to metastasize to all sites, they display an increased ability to colonize the site from which they were isolated (Rose et al., 2007, 2010; Tabariès et al., 2011) (Figure 2A). Using gene expression profiling data generated from parental 4T1 cells and each of these site-selective metastatic cell populations, we assembled a composite metabolic gene expression signature based on KEGG designations (Table S1). Using this composite metabolic signature, we observed a distinct gene expression pattern in liver-metastatic 4T1 subpopulations (2776 and 2792) relative to parental 4T1, bone-metastatic (592 and 593), and lung-metastatic (533 and 537) cells (Figure 2B). Liver-metastatic 4T1 cells displayed enrichment for genes encoding components of the glycolytic pathway (Figure 2C), including Aldolase, Lactate dehydrogenase, Phosphofructokinase, Glucose phosphate isomerase, and Enolase (Table S2), while displaying reduced expression of genes involved in the TCA cycle and OXPHOS (Figure 2D; Table S3).

We next conducted SITA using U-[^{13}C]-glucose on the organ-selective metastatic cell populations (bone, lung, and liver), and found differences in glucose utilization depending on the metastatic site. For these experiments, we pulsed cells with U-[^{13}C]-glucose for 30 min and displayed the averaged data of two independent explant populations for each metastatic site. Overall pyruvate abundance was elevated in all organ-selective metastatic populations relative to parental 4T1 cells (Figure S2A), with ^{13}C incorporation corresponding to the m+3 isotopomer (Figure S2B). Taking into account both the metabolite pool size and ^{13}C enrichment in each pool, we found that bone-metastatic cells displayed an increase in the total amount of U-[^{13}C]-glucose-labeled pyruvate, while the production of U-[^{13}C]-glucose-derived pyruvate in lung and liver-metastatic cells was similar to parental 4T1 cells (Figure 2E). Overall, lactate pools were elevated in all metastatic explants compared to parental 4T1 cells (Figure S2C); however, liver-metastatic breast cancer cells displayed a specific increase in labeling of lactate from U-[^{13}C]-glucose (Figures 2F, S2C, and S2D). Bone- and lung-metastatic cell populations displayed an increase in both total citrate abundance and levels of glucose-derived citrate compared to parental 4T1 cells (Figures 2G and S2E). Conversely, liver-metastatic cells displayed a slight decrease in the levels of glucose-derived citrate relative to parental 4T1 cells (Figures 2G), corresponding to an increase in the abundance of the m+0 isotopomer in liver-metastatic cells, along with a decrease in the m+2 isotopomer (Figures S2E and S2F).

To confirm these results, we performed SITA experiments using a shorter labeling period (15 min pulse with U-[^{13}C]-glucose) on the individual liver-metastatic cell lines (denoted 2776 and 2792). We observed that, while the total pyruvate pool did not significantly change (Figure S2G), the fraction of pyruvate derived from U-[^{13}C]-glucose was increased in the liver-metastatic cells compared to parental 4T1 cells (Figure S2G), resulting in an increased abundance of labeled lactate (Figure 2H). Similarly, we observed an increase in the overall lactate pool (Figure S2H) as well as the fraction derived from U-[^{13}C]-glucose (72% and 79% relative to 43%). This analysis revealed elevated levels of glucose-derived lactate in liver-metastatic cells compared to parental 4T1 cells (Figures 2I and S2H). In contrast, we observed a significant reduction in both the fraction (Figures S2I–S2L) and abundance of U-[^{13}C]-glucose-derived citrate (Figure 2J) in 2776 and 2792 liver-metastatic cells, while the total pool was only slightly decreased (Figure S2I). Isotopomer labeling patterns for pyruvate, lactate, and citrate in liver-aggressive metastatic cells were in agreement with our earlier observations (Figures S2J–S2L). Together, these data indicate that breast cancer cells display distinct metabolic signatures depending on the metastatic site.

Liver-Metastatic Breast Cancer Cells Display Reduced Glutamine Metabolism and OXPHOS

Another aspect of aggressive cancer cells that display the Warburg effect is increased glutamine metabolism (DeBerardinis et al., 2007). Glutamine is a key anaplerotic substrate for the TCA cycle through its conversion to α-ketoglutarate (α-KG) (Figure S3A) (Hensley et al., 2013). To assess differences in

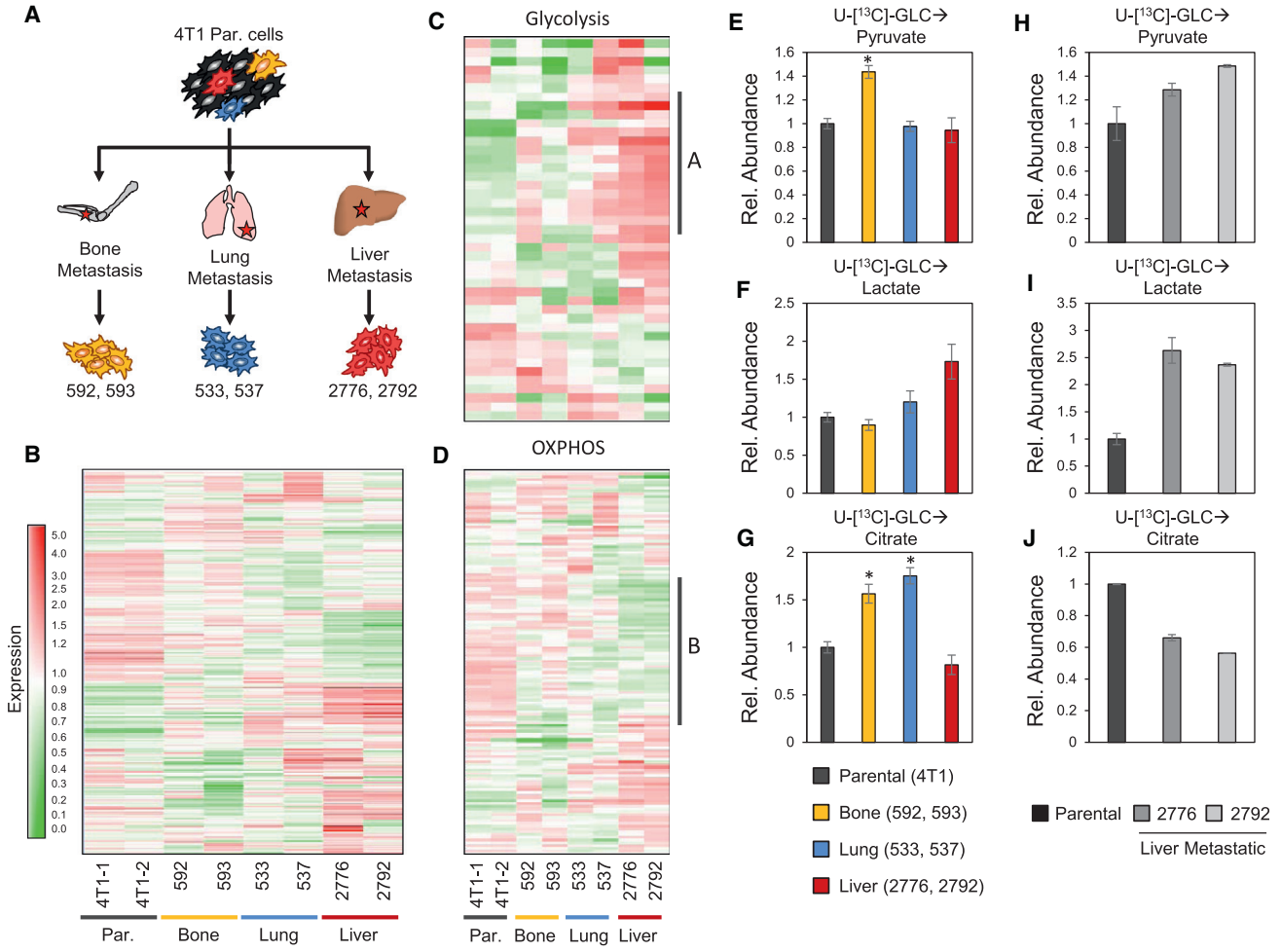

Figure 2. Organ-Selective Metastatic Breast Cancer Cells Display Differential Glucose Utilization

(A) Schematic depicting the origin of in vivo selected metastatic breast cancer cell populations.

(B) The expression level of 680 genes, representing major cellular metabolic pathways (Table S1), was compared between the parental 4T1 and the various organ-selective metastatic cell populations.

(C and D) (C) Genes in the glycolysis (43 genes) and (D) OXPHOS pathways (136 genes) are shown in detail. The identity of genes corresponding to areas A and B of the heatmaps are listed in Tables S2 and S3, respectively.

(E–J) SITA measuring the conversion of U-[^{13}C]-glucose into pyruvate (E and H), lactate (F and I), and citrate (G and J). The data represent abundance of the labeled portion of the indicated metabolite relative to 4T1 cells. (E–G) Organ-selective metastatic cell populations and 4T1 parental cells were pulsed with U-[^{13}C]-glucose for 30 min and the presented data correspond to the average of two independent cell populations each performed in duplicate. (H–J) Liver-metastatic cell populations and 4T1 parental cells were pulsed with U-[^{13}C]-glucose for 15 min. (E) *p < 0.05 (SD); (G) *p < 0.05 (SD).

glutamine utilization by organ-selective metastatic breast cancer cells, two independent explant populations from each metastatic site were cultured with U-[^{13}C]-glutamine for 30 min and TCA cycle metabolites analyzed using GC-MS. Bone- and lung-metastatic populations displayed increased U-[^{13}C]-glutamine uptake and total glutamine pools relative to 4T1 parental cells (Figures 3A and S3B), as well as increased abundance of U-[^{13}C]-glutamine-derived TCA cycle intermediates including succinate (Figures 3B and S3C) and citrate (Figures 3C and S3D; left panel). In contrast, glutamine uptake in liver-metastatic cells was similar to parental 4T1 cells (Figures 3A and S3B), and the levels of total and glutamine-derived TCA cycle metabolites were either reduced (succinate, Figures 3B and S3C) or unchanged (citrate, Figures 3C and S3D; left panel) in liver-metastatic subpopulations compared to parental 4T1 cells. However, the overall fractions of the total pool for each metabolite labeled from glutamine were similar in all cell populations (Figure S3). Analysis of the individual liver-metastatic populations (2776 and 2792) revealed additional differences compared to the parental 4T1 cells with a further shift away from oxidative glutamine metabolism. We observed a 60% reduction in glutamine pools in the 2776 and 2792 liver-metastatic cells compared to parental 4T1 cells (Figures 3D and S3E), which translated into a decrease in total pools and [^{13}C]-glutamine-derived abundance of the TCA cycle intermediates succinate, citrate, fumarate, malate and aspartate (Figures 3E–3I and S3F–S3J).

Cancer cells with diminished mitochondrial activity often engage reductive carboxylation (schematic in Figure S3A) to

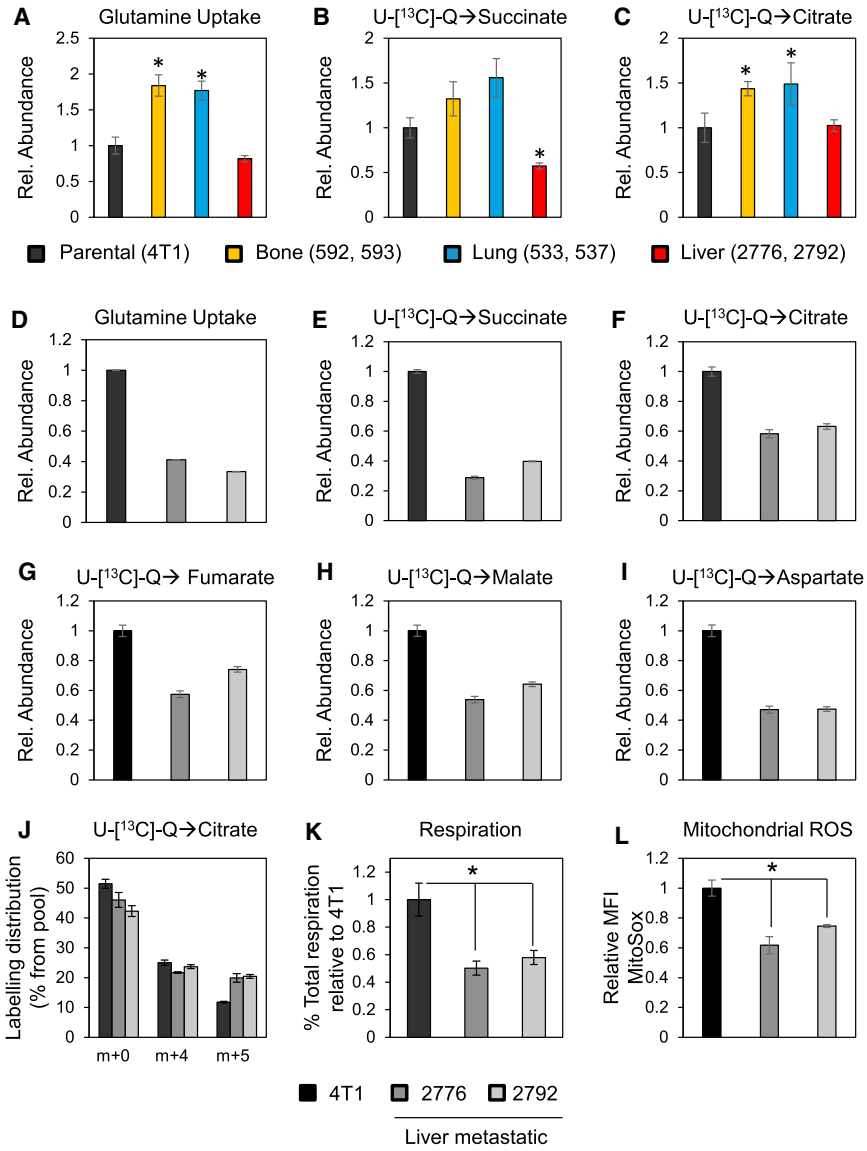

Figure 3. Liver-Metastatic Breast Cancer Cells Display Reduced Oxidative Glutamine Metabolism and Oxidative Phosphorylation

Measurement of glutamine uptake into cells (A and D) and its conversion into succinate (B and E), citrate (C and F), fumarate (G), malate (H), and aspartate (I). Data represent the abundance of the labeled portion of the indicated metabolite relative to 4T1 cells.

(A–C) Organ-selective metastatic cell populations and 4T1 parental cells were pulsed with U-[^{13}C]-glutamine for 30 min. Data correspond to the average of two independent cell populations, each performed in duplicate.

(D–F) The same experiment was repeated in the liver-metastatic cell populations and 4T1 parental cells, and each graph represents the data for a single cell population performed in duplicate.

(J) The graph represents the distribution of the [^{13}C] label between the m+4 and m+5 isoforms of citrate.

(K) Total cellular respiration was assayed for the liver-metastatic cells lines. The data correspond to an average of five experiments and are expressed as a fold change relative to 4T1 cells.

(L) Mitochondrial-specific ROS were analyzed using MitoSox and are plotted as a fold change relative to 4T1 cells.

(A) *$p < 0.05$ (SD); (B) *$p < 0.05$ (SD); (C) *$p < 0.05$ (SD); (K) *$p < 0.05$ (SEM); (L) *$p < 0.05$ (SEM).

bolism is reduced in liver-metastatic breast cancer cells, while glutamine anaplerosis is a salient feature of lung- and bone-metastatic cells.

HIF-1α Mediates Metabolic Reprogramming of Liver-Metastatic Breast Cancer Cells

HIF-1α is a master transcription factor that controls metabolic reprogramming under low-O_2 conditions, and it functions as a key regulator of glycolysis (Keith et al., 2012; Semenza, 2013). We assessed HIF-1α activity in metastatic breast cancer cells using a reporter system comprised of HIF responsive elements (HRE) controlling luciferase expression (Yan et al., 2014). HIF-1α transcriptional activity was elevated under normoxic conditions in liver-metastatic cell populations and could be further induced under hypoxic conditions (Figure 4A). Despite no evidence of increased HIF-1α protein expression (Figure 4B), liver-metastatic cells (2776 and 2792) displayed modestly elevated expression of *Hif-1α* mRNA and a significant increase in expression of HIF-1α-dependent target genes, including major enzymes of the glycolytic pathway (Figure 4C).

To assess the contribution of HIF-1α to the observed metabolic program, two independent shRNAs were used to silence HIF-1α protein expression in 2776 and 2792 liver-metastatic cell populations (Figure 4D). SITA using U-[^{13}C]-glucose revealed no major changes in the relative abundance of labeled pyruvate generated from U-[^{13}C]-glucose between parental

generate glutamine-derived acetyl-CoA that contributes to biosynthetic pathways such as lipid biosynthesis (Metallo et al., 2012). Liver-metastatic cells exhibited a 40% increase in reductive carboxylation (as indicated by increased m+5 citrate in 2776 and 2792 cells) compared to parental 4T1 cells (Figure 3J), suggesting differences in carbon flow in these cell populations. Interestingly, levels of the m+5 citrate isotopomer in bone- and lung-metastatic cells did not differ from that seen in parental 4T1 cells (Figure S3D; right panel).

Finally, we assessed the impact of reduced carbon flow into the TCA cycle on rates of OXPHOS in liver-metastatic cells. Liver-metastatic breast cancer cells (2776 and 2792) displayed a 40%–50% reduction in total respiration relative to parental cells (Figure 3K). One expected consequence of lower mitochondrial activity is reduced production of reactive oxygen species (ROS). Levels of mitochondrial ROS were 30%–40% lower in liver-metastatic cells compared to parental 4T1 cells (Figure 3L). Together, these data indicate that oxidative glutamine meta-

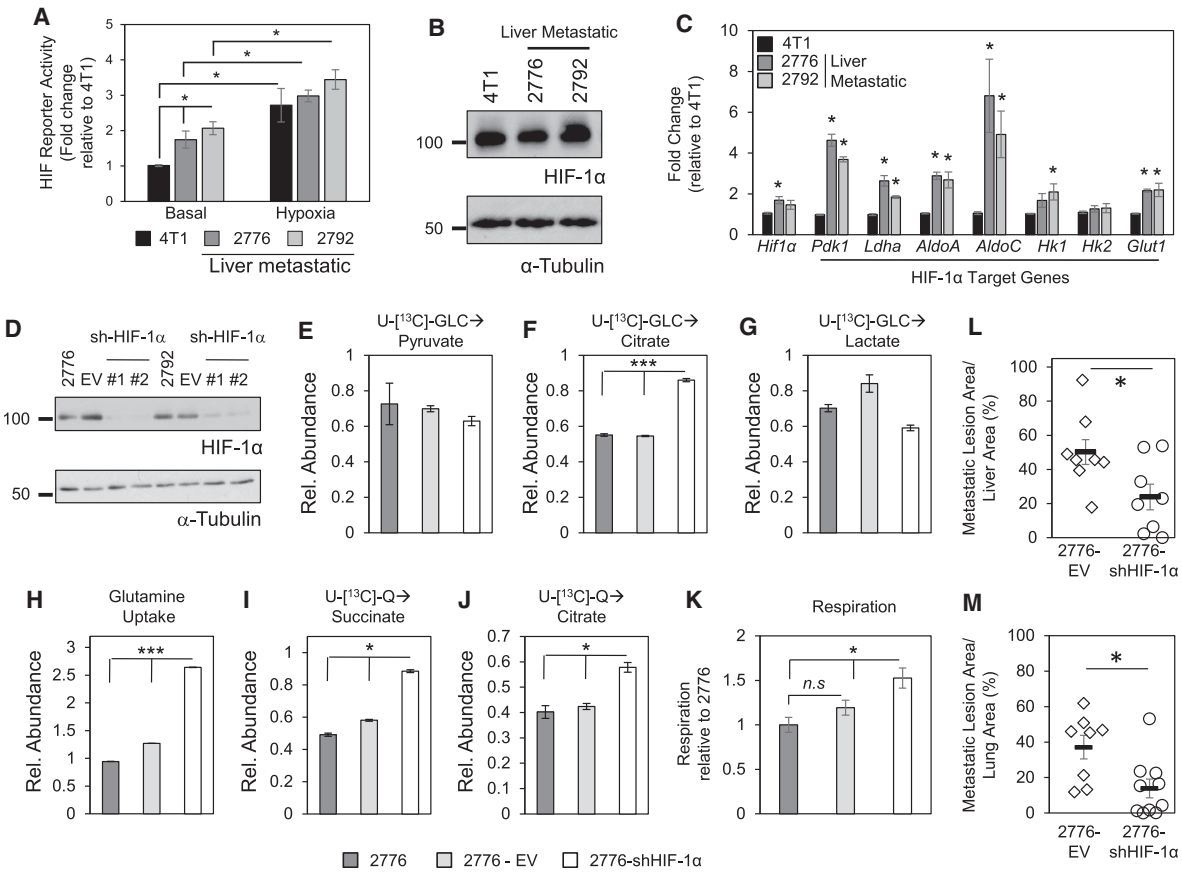

Figure 4. HIF-1α Is Hyperactivated in Liver-Metastatic Breast Cancer Cells and Partially Drives Metabolic Reprogramming

(A) HIF-1 transcriptional activity under basal and hypoxic conditions. The data correspond to an average of three experiments performed in duplicate.

(B) Immunoblot analysis of HIF-1α in 4T1 parental cells and the liver-metastatic 4T1 subpopulations. α-Tubulin served as a loading control.

(C) Expression levels of HIF-1α and known HIF target genes were analyzed by RT-qPCR. The data represent an average of two independent experiments, each performed in duplicate.

(D) Immunoblot analysis to assess efficiency of HIF-1α knockdown. α-Tubulin served as a loading control.

(E–J) SITA using U-[^{13}C]-glucose for 15 min (E–G) or U-[^{13}C]-glutamine for 30 min (H–J). The data represent the abundance of the [^{13}C] incorporated into pyruvate (E), lactate (F), and citrate (G) derived from glucose; or the labeled glutamine within the cells (H) and its incorporation into succinate (I) or citrate (J).

(K) Total cellular respiration was measured in 2776, vector control, and HIF-1α KD cells. The data correspond to an average of three experiments and are expressed as a fold change relative to 2776 cells.

(L and M) Quantification of the metastatic burden in the liver (L) and the lung (M) following injection with control and HIF-1α KD cells (n = 8 for splenic injections of 2776-EV and 2776-shHIF-1α; n = 8 for tail vein injections of 2776-EV and n = 9 for 2776-shHIF-1α).

(A) *p < 0.05 (SEM); (C) *p < 0.05 (SD); (F) ***p < 0.001 (SD); (H) ***p < 0.001 (SD); (I) *p < 0.05 (SD); (J) *p < 0.05 (SD); (K) *p < 0.05 (SEM); (L) *p < 0.05 (SEM); (M) *p < 0.05 (SEM).

liver-aggressive cells and those expressing a control vector (EV) or HIF-1α-specific shRNA (shHIF-1α) (Figure 4E). However, silencing HIF-1α in liver-aggressive cells effectively reversed the fate of pyruvate in these cells, as evidenced by an increase in the abundance of [^{13}C]-glucose-derived citrate (Figure 4F) and a decrease in [^{13}C]-glucose-derived lactate (Figure 4G). Silencing HIF-1α promoted increased [^{13}C]-glutamine uptake by liver-metastatic cells (Figure 4H), as well as an increase of [^{13}C]-glutamine-derived TCA cycle metabolites including succinate (Figure 4I) and citrate (Figure 4J). Finally, we observed a significant increase in respiration in liver-metastatic cells expressing HIF-1α shRNAs compared to control populations (Figure 4K). These results suggest that HIF-1α is a major driver of the metabolic phenotype (glycolysis > OXPHOS) in the liver-metastatic explant populations studied here.

We next determined the importance of the HIF-1α pathway for the metastatic potential of these breast cancer cells. Experimental metastasis assays were performed by injecting HIF-1α knockdown (KD) and empty vector (EV) control cells into either the spleen or the tail vein, and colonization of the liver (Figure 4L) and lungs (Figure 4M), respectively, was assessed. Silencing HIF-1α impaired the capacity of the breast cancer cells to metastasize to both sites, resulting in a 50% reduction of the metastatic burden in the lungs and liver relative to controls.

PDK1 Mediates Adaption to Metabolic Stress in Liver-Metastatic Breast Cancer Cells

Pyruvate dehydrogenase kinase-1 (PDK1) is a HIF-1α target that antagonizes the function of Pyruvate dehydrogenase (PDH), a key rate-limiting enzyme for pyruvate conversion to acetyl-coA

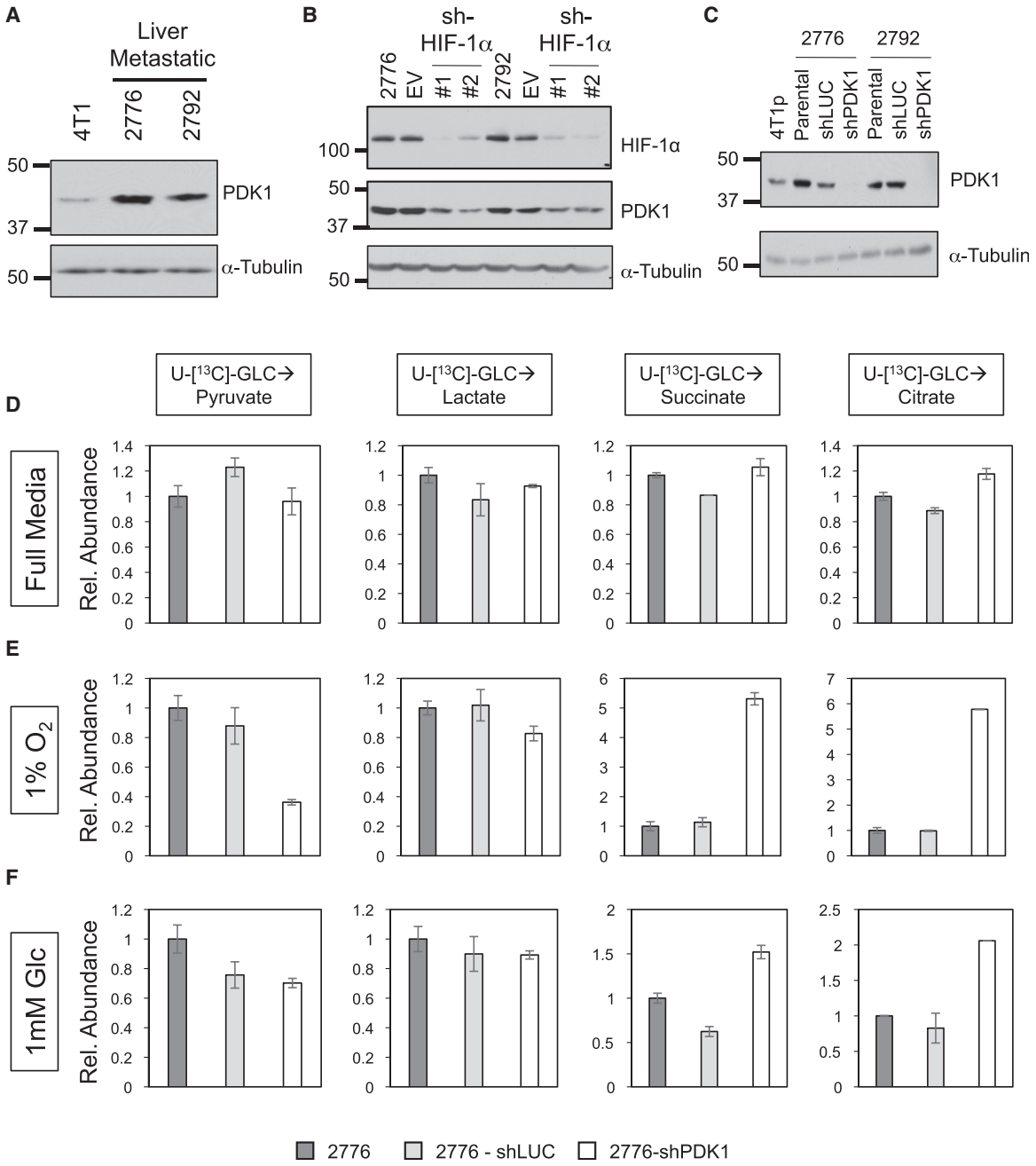

Figure 5. PDK1 Is Required for Metabolic Adaption of Breast Cancer Cells in Response to Stress

(A) Immunoblot analysis of PDK1 levels in liver-metastatic breast cancer cells compared to 4T1 parental cells.

(B) Immunoblot analysis of HIF-1α and PDK1 in the liver-metastatic breast cancer cells following HIF-1α KD.

(C) Immunoblot analysis showing the efficiency of PDK1 KD in the liver-metastatic 4T1 subpopulations. α-Tubulin served as a loading control (A–C).

(D–G) SITA measuring the conversion of U-[^{13}C]-glucose into pyruvate, lactate, succinate, and citrate in regular growth media (D) or cultured 24 hr either with 1% O_2 (E) or 1 mM glucose (F). Data represent relative abundance of the labeled portion of the indicated metabolite for one representative experiment performed in duplicate.

and entry into the TCA cycle. PDK1-dependent inhibition of PDH reduces the conversion of pyruvate to acetyl-CoA, leading to reduced flow of glucose-derived pyruvate into the TCA cycle, especially under hypoxic conditions (Kim et al., 2006; Papandreou et al., 2006). Consistent with the 4-fold increase in *Pdk1* mRNA expression seen in liver-metastatic explants (Figure 4C), we observed increased PDK1 protein levels in the 2776 and 2792 liver-aggressive populations compared to parental 4T1 cells (Figure 5A). PDK1 expression in these cells was dependent on HIF-1α, as PDK1 protein levels were reduced in liver-metastatic cells expressing HIF-1α shRNAs (Figure 5B). The functional consequences of reduced HIF-1α levels, causing

diminished PDK1 expression, was revealed by impaired serine phosphorylation of PDH on residue 203 (Site 3), a PDK1-specific phosphorylation site (Figure S4A).

It is conceivable that variable levels of PDK1 exist in the parental 4T1 cell population and are selected for following seeding of the liver. Alternatively, PDK1 expression may be absent in the parental population and induced following colonization of the liver and growth of hepatic metastases. PDK1 immunohistochemical staining of primary mammary tumors derived from parental 4T1 cells revealed variable PDK1 expression in 4T1 tumors (Figure S4B). In addition, we isolated several clonal populations derived from parental 4T1 cells and assessed PDK1 protein expression. The expression of PDK1 in 4T1 cell clones was diverse, with some clones negative for PDK1 and others exhibiting levels comparable to the 2776 liver-metastatic population (Figure S4C). These data argue that a pre-existing population of PDK1-expressing cells is likely selected for during the formation of liver metastases.

The contribution of PDK1 to the metabolic reprogramming of liver-metastatic cell populations was next assessed through shRNA-mediated silencing of PDK1 (Figure 5C). Surprisingly, under normal culture conditions we observed no differences in the ECAR, OCR, or total respiration rates of PDK1 shRNA-expressing liver-metastatic 2776 cells (2776-shPDK1) relative to parental cells or 2776 cells expressing a control shRNA targeting luciferase (2776-shLUC) (Figures S4D–S4F). Similarly, unlike their counterparts expressing HIF-1α shRNAs, liver-metastatic cells expressing PDK1 shRNAs did not display significant changes in levels of [^{13}C]-glucose-derived lactate, succinate, or citrate (Figure 5D). However, PDK1 was required for Ser-203 PDH phosphorylation under both normoxic and hypoxic conditions (Figure S4G), and was required to mediate metabolic adaptations to low oxygen (1% O_2) or low glucose (1 mM). Liver-metastatic cells expressing PDK1 shRNA displayed a dramatic reduction in the abundance of [^{13}C]-glucose-derived pyruvate under hypoxia (Figure 5E). This did not correlate with changes in intracellular lactate production under hypoxia; rather, 2776-shPDK1 cells displayed a striking increase in levels of [^{13}C]-glucose-derived succinate and citrate in response to hypoxia (Figure 5E), consistent with increased pyruvate flow into the TCA cycle. Conversely, low-glucose conditions did not affect the relative abundance of labeled pyruvate or lactate in liver-metastatic cells, but specifically promoted the accumulation of [^{13}C]-glucose-derived succinate and citrate in liver-metastatic cells expressing PDK1 shRNA (Figure 5F). Thus, PDK1 expression appeared to alter the flow of ^{13}C-glucose carbon to the TCA cycle specifically under low-oxygen and low-glucose conditions.

PDK1 Expression Is Required for Efficient Breast Cancer Liver Metastasis

We next assessed the impact of silencing PDK1 expression on the ability of liver-metastatic cells to grow as primary tumors or form liver metastases. Parental 2776 or 2792 liver-metastatic cells, or liver-metastatic cells expressing control shRNA (shLUC) or shRNA targeting PDK1 (shPDK1), were injected into the mammary fat pad of Balb/c mice and primary tumor growth assessed over time. We observed no statistically significant differences in primary mammary tumor growth between mice injected with parental, shLUC-expressing, or shPDK1-expressing 2776 (Figure 6A) or 2792 (Figure 6B) cell populations. To test the impact of silencing PDK1 on the liver-metastatic phenotype of these cells, we performed experimental metastasis assays via splenic injection. Three weeks postinjection, livers from recipient mice were harvested and the metastatic burden quantified. We observed an 80% reduction in liver metastatic burden in mice that received 2776-shPDK1 or 2792-shPDK1 cells compared to mice that had received parental or shLUC-expressing liver-metastatic cells (Figures 6C and 6D). Histological examination of livers from these mice revealed a reduction in both the number and size of metastatic lesions originating from 2776-shPDK1 or 2792-shPDK1 cells (Figures 6E and 6F). These data suggest that PDK1 is required for the formation of efficient liver metastases in this model.

To better define the stage during breast cancer cell seeding and colonization of the liver that is dependent on PDK1 function, we performed a short-term seeding assay using CFSE-labeled 2776-shLUC and 2776-shPDK1 cells and assessed the number of cells present in the liver post-splenic injection. Two hours postinjection (day 0), the labeled tumor cells remained within the liver sinusoids, with few extravasated cells visible in either cohort (Figure S5A). Similar numbers of extravasated breast cancer cells were quantified at 26 (day 1) and 50 (day 2) hours postinjection, revealing that the significant reduction in liver-metastatic burden observed in cells lacking PDK1 (Figure 6) was not due to a defect in the extravasation potential of the cells (Figure S5A). To determine if reduced PDK1 expression affects general metastatic potential, we assessed metastatic burden in the lung following tail vein injections of the 2776-shLUC and 2776-shPDK1 cells. Interestingly, reduced PDK1 levels did not affect the ability of breast cancer cells to form lung metastases (Figure S5B), even though the ability to form liver metastases was severely impaired (Figure 6). These data argue that the importance of PDK1 in the metastatic process becomes evident following tumor cell adaptation to the liver microenvironment.

PDK1 Expression Is Elevated in Liver Metastases from Breast Cancer Patients

To further study the role of PDK1 in human metastatic breast cancer, we investigated its level of expression by immunohistocytochemistry in a breast tumor microarray containing 330 tumor cores that were linked to clinical outcomes. Of these cores, 282 could be scored for PDK1 expression. We saw no association between high levels of PDK1 expression in the primary breast tumor and breast cancer-specific patient survival (Figures S6A and S6B). Next, we assessed PDK1 expression by IHC in liver metastases from nine breast cancer patients as well as seven matched primary breast tumor sections (Figure 7). Analysis of these tumor sections revealed considerable variability in PDK1 expression in primary breast tumors, but consistent increases in PDK1 staining (either signal intensity or percentage positivity of PDK1 staining) in liver metastases compared to matched primary tumors in all seven patients examined. Two additional liver metastases from breast cancer patients, for which insufficient tumor cells could be identified in the primary tumor, also revealed higher PDK1 signal compared to the average intensity found in the other primary tumors. To determine if PDK1 expression was elevated in all metastases, regardless of site, we

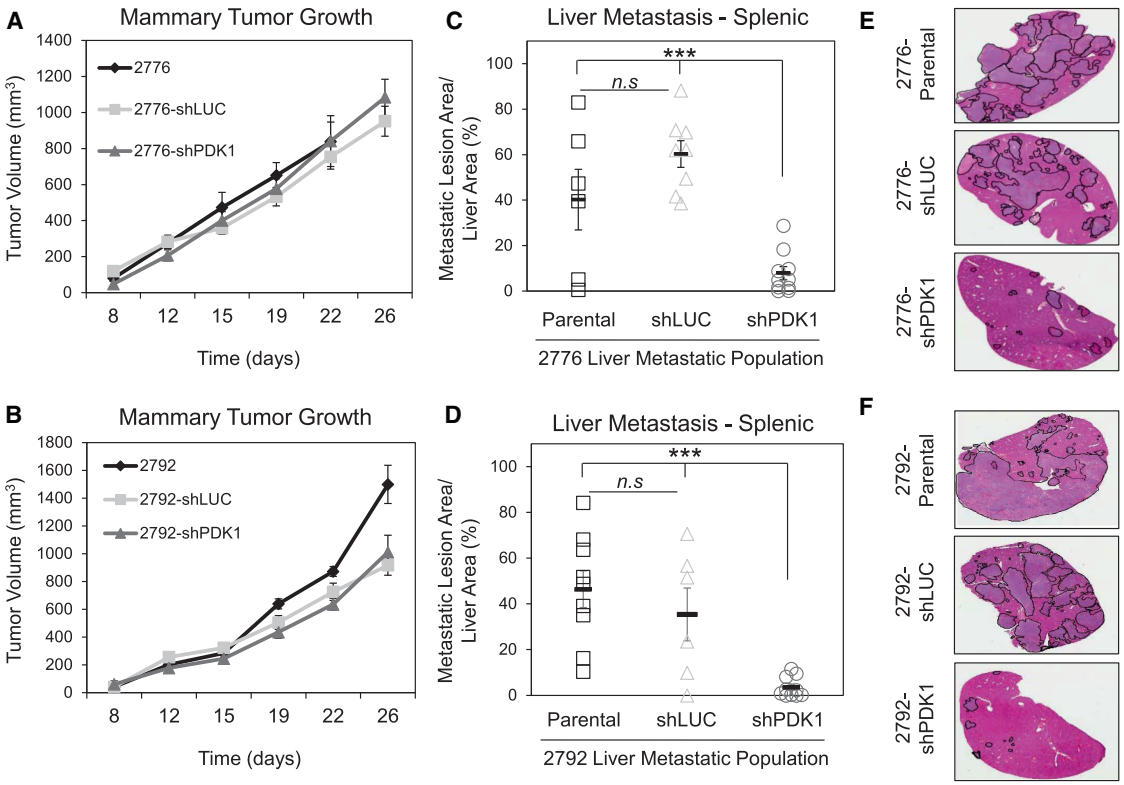

Figure 6. PDK1 Expression Is Critical for Efficient Breast Cancer Liver Metastasis

(A and B) Tumor growth following mammary fat pad injections of parental, control and PDK1 KD cells in either 2776 (A) or 2792 (B) breast cancer populations. (C and D) Liver-metastatic burden was calculated following splenic injections of the 2776 (C) or 2792 (D) populations (n = 6 for 2776, n = 8 for 2776-shLUC, n = 10 for 2776-shPDK1, n = 9 for 2792, n = 6 for 2792-shLUC and n = 10 for 2792-shPDK1). (C) ***p < 0.001 (SEM); (D) ***p < 0.001 (SEM).

(E and F) Representative images of liver sections stained with H&E. (***p < 0.001).

analyzed the PDK1 expression in five matched primary breast tumors and skin metastases. Interestingly, we did not observe an increase in PDK1 staining in skin metastases compared to their matched primary tumors (Figure S6C). Together these data suggest an important role for PDK1 in mediating liver metastasis in human breast cancer.

DISCUSSION

Renewed attention has been focused on altered metabolism that accompanies tumor initiation and growth in the primary site (Ward and Thompson, 2012). However, there have been conflicting opinions regarding the metabolic programs that underpin the metastatic process in breast cancer. Previous efforts to define the metabolic profiles of metastatic breast cancer cells revealed a progressive shift toward a glycolytic phenotype as normal mammary epithelial cells progress to non-metastatic breast cancer, with further changes in both glycolytic and OXPHOS metabolite levels in metastatic breast cancer (Lu et al., 2010). The authors concluded that no further metabolic changes correlated with the acquisition of increasing metastatic activity (Lu et al., 2010). Others have identified OXPHOS and increased mitochondrial activity as important contributors to the metastatic phenotype (LeBleu et al., 2014; Porporato et al., 2014). Here we demonstrate that breast cancer cells transitioning to the metastatic state display increases in both OXPHOS and glycolysis, but that additional, distinct metabolic changes are associated with site-specific metastases. Our data suggest that breast cancer cells with broad metastatic potential (4T1—bone, lung, and liver) engage both OXPHOS and glycolysis, while cells with site-selective metastatic potential engage OXPHOS (bone or lung-metastatic cells) or glycolysis-dependent (liver-metastatic cells) metabolic strategies. We demonstrate that liver-specific metastatic breast cancer cells are specifically programmed—via HIF-1α, and PDK1—to maintain their glycolytic phenotype, and that PDK1 is required for these breast cancer cells to successfully metastasize to the liver. The emergence of elevated PDK1 levels in liver metastases from breast cancer patients, even in patients with low PDK1 expression in their primary tumors, suggests that active shifts in metabolic reprogramming may contribute to metastatic progression in human disease.

In our model, metastatic breast cancer populations (66cl4, 4T1 cells) displayed elevated OXPHOS and TCA cycle activity compared to non-metastatic cell variants (67NR), with highly metastatic 4T1 cells also displaying significant increases in glycolytic metabolism. Other groups have found a similar shift toward mitochondrial metabolism in metastatic cells (LeBleu et al., 2014; Porporato et al., 2014). For example, PGC-1α-dependent increases in mitochondrial biogenesis, respiration, and oxidative capacity are required for 4T1 cells to effectively form lung

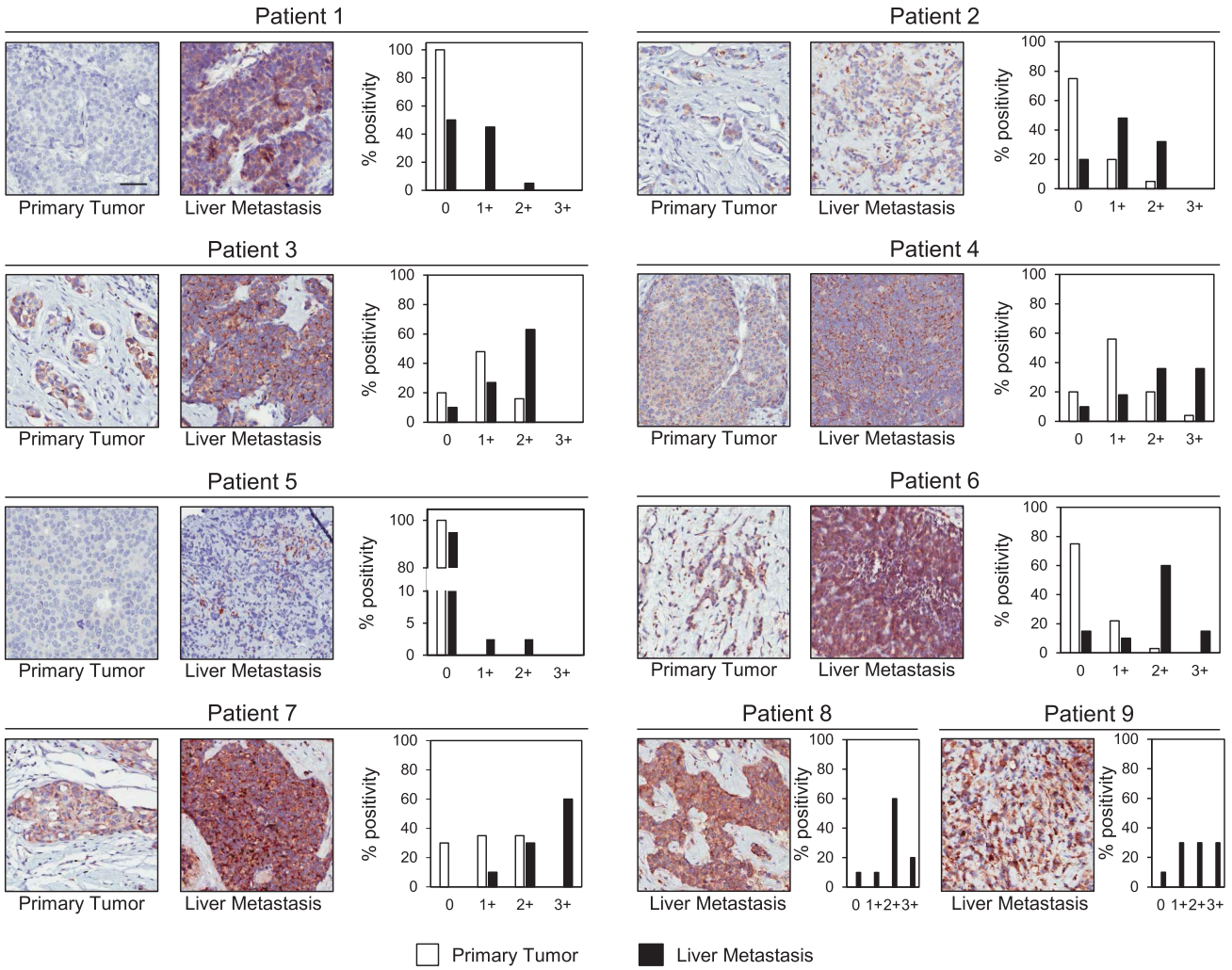

Figure 7. PDK1 Expression Is Elevated in Liver Metastases Derived from Patients with Breast Cancer Relative to Matched Primary Breast Tumors

Representative images of PDK1 staining in primary human breast tumors and matched liver metastases are shown. The scale bar represents 50 μm and applies to all panels. Graphs corresponding to the quantification of PDK1 staining and representing the percentage positivity as well as the staining intensity (0 = negative, 1 = weak, 2 = moderate, and 3 = strong) in both the primary tumors (white bars) and liver metastases (black bars) are presented.

metastases (LeBleu et al., 2014). However, our work also suggests that breast cancer cells with similar genetic backgrounds, but with preferential metastatic tropism to different sites, display distinct metabolic profiles. Our data suggest that a bifurcation of metabolic programs between OXPHOS (favored by lung and bone metastases) and glycolytic metabolism (liver metastases) may define metastatic fitness to specific sites, leading to the discrepancy between these studies. These data are in agreement with recent work demonstrating that the metabolic profile of tumor cells depends not only on the driving oncogenes but also on the tissue type (Yuneva et al., 2012).

Our data highlight a key role for HIF-1α and PDK1 in the glycolytic program engaged by liver-metastatic breast tumor cells. Interestingly, while HIF-1α appeared to be a master regulator of the metabolic phenotype under basal conditions, PDK1 was specifically required for metabolic adaptation in response to metabolic stress. The reduction of both lung and liver metastasis in breast cancer cells harboring reduced HIF-1α levels also supports a broader functional role for this transcription factor in the metastatic process. In contrast, reduced PDK1 expression appears to play a more restricted role in controlling the metabolic fitness of cancer cells under metabolic stress associated with certain microenvironments.

Contradictory data exist with respect to the role of the PDKs in regulating tumor metabolism and growth. PDK1 was originally characterized as a key inhibitor of pyruvate entry into the TCA cycle under hypoxic growth conditions (Kim et al., 2006; Papandreou et al., 2006). Our data indicate that silencing PDK1 in liver-metastatic breast cancer cells has no effect on basal tumor metabolism and primary tumor growth. Rather, we find that, under conditions of limited oxygen or glucose, reducing PDK1 expression in metastatic breast cancer cells dramatically affects their ability to use glucose as mitochondrial fuel sources. Several studies argue that PDK1 inhibition is sufficient to revert the

glycolytic phenotype leading to increased mitochondrial respiration and altered tumor growth (Bonnet et al., 2007; Sutendra et al., 2013). However, it is important to note that many of these studies employed dichloroacetate (DCA) as a PDK inhibitor. In addition to inhibiting PDK-dependent PDH phosphorylation, DCA can also reduce HIF-1α levels (Kumar et al., 2012; Sutendra et al., 2013) and induce oxidative stress responses (Hassoun and Ray, 2003). Thus, the antitumor effects of DCA treatment may not be solely due to its effects on PDK activity. Our results argue that PDK1 is required to mediate the adaptability of liver-metastatic breast cancer cells to better deal with stresses encountered during metastatic dissemination, such as the adaptation to a new microenvironment. In agreement with this, we show that PDK1 expression is enhanced in liver metastasis of breast cancer patients compared to their matched primary tumor. Interestingly, a similar increase is not observed in skin metastases relative to matched primary breast tumors.

One question that arises from our work is, why is the metabolic program of liver-specific metastatic cells different than those that colonize different sites? Indeed, bone- and lung-specific metastases directed pyruvate into the TCA cycle to support OXPHOS and mitochondrial-dependent biosynthesis, while liver-metastatic breast cancer cells preferentially converted pyruvate into lactate, characteristic of the Warburg effect. Similarly, liver-aggressive cells displayed reduced levels of glutamine oxidation, and increasingly generated glutamine-derived citrate for biosynthesis via reductive carboxylation. Thus, while the bioenergetic and biosynthetic requirements of all metastatic populations are met, the liver-metastatic cells achieved this through different metabolic programs. In this context, liver-metastatic breast cancer cells have adopted a metabolic profile similar to that of cells grown under hypoxia. In addition to increased glycolysis and reduced TCA cycle activity, hypoxia or pseudohypoxia was shown to reduce glutamine oxidation and favor reductive carboxylation to produce citrate through HIF-dependant induction of Isocitrate dehydrogenase (IDH) and bypass of the mitochondrial-dependent production of acetyl-CoA from glutamine for de novo lipogenesis (Metallo et al., 2012; Wise et al., 2011). Alternatively, it has been shown that HIF-1 stabilization diminishes the conversion αKG to succinate through loss of OGDH2, a subunit of the αKG dehydrogenase (αKGDH) complex (Sun and Denko, 2014). Under these conditions, glutamine undergoes reductive carboxylation to produce citrate for lipid synthesis (Sun and Denko, 2014). Our data suggest that the HIF-1α-dependent metabolic signature displayed by the liver-metastatic breast cancer cells is already present in subsets of cells that comprise the parental 4T1 population. Altogether, this suggests a potential selection for metastatic cells that have gained additional mutations or epigenetic changes that favor the metabolic programs required for successful metastasis to specific sites. In addition, our short-term metastasis assay suggests that the impaired metastatic potential of tumor cells lacking PDK1 results from growth defects within the liver rather than a deficiency in the initial seeding of the organ.

By virtue of its function as a gluconeogenic tissue, the liver may provide a conducive microenvironment for metastatic breast cancer cells whose growth is fueled by glycolysis. Our data show that metastatic breast cancer cells isolated from the liver exhibit high levels of glycolytic metabolism and lactate production. Hepatocytes may take up lactate (or other tumor-derived metabolites) and convert them into other metabolites that can then feed back to cancer cells to fuel their growth. Metabolic coupling of cancer cells and non-transformed stromal cells is observed in ovarian cancer, where adipocytes can transfer lipids to adjacent tumor cells to fuel OXPHOS (Nieman et al., 2011). In this light, we speculate that liver-metastatic breast cancer cells are metabolically coupled to hepatocytes on the basis of glucose availability, and that HIF-1α and PDK1 help confer compatibility of these tumor cells with the liver. Understanding the metabolic codependencies of metastatic breast cancer cells with their local microenvironments may reveal potential vulnerabilities suitable for therapeutic targeting.

EXPERIMENTAL PROCEDURES

Cell Lines, Cell Culture, and DNA Constructs

67NR, 66cl4, and 4T1 cell lines were cultured as previously described (Rose et al., 2007). The 4T1-derived liver-aggressive (2776 and 2792), lung-aggressive (533 and 537), and bone-aggressive cell populations (592 and 593) were described previously (Tabariès et al., 2015). Proliferation rates were determined by seeding cells in 6-well plates and performing cell counts every day over a 4-day period to determine population doublings. ROS levels were measured using MitoSOX Red mitochondrial superoxide indicator (Invitrogen, #M36008) following a 15 min incubation period, and Mean Fluorescence Intensity (MFI) determined by flow cytometry. HIF-1α knockdown was achieved using lentiviral shRNA vectors from the TRC shRNA collection (Sigma-Aldrich, St. Louis, MO; TRCN0000232220 [hp#1] and TRCN0000232222 [hp#2]). Lentiviral supernatants were generated as described (Huang et al., 2012). PDK1 knockdown was achieved using the miR-30-adapted LMP retroviral vector system (Dickins et al., 2005).

Metabolic Assays

Glucose consumption and lactate production were measured using a Nova BioProfile 400 (Nova Biomedical, Mississauga, ON, Canada) using established protocols (Dupuy et al., 2013; Faubert et al., 2014). ECAR and OCR were measured using an XF24 or XF96 Extracellular Flux Analyzer (Seahorse Bioscience, North Billerica, MA, USA) as previously described (Dupuy et al., 2013). Respiration measurements were performed using a Digital Model 10 Clarke Electrode (Rank Brothers, Cambridge, UK). Total respiration was determined for 1×10^6 cells, and maximal respiratory capacity was determined after the addition of FCCP (1.5 μM).

GC-MS Analysis of ^{13}C Metabolites

GC-MS and SITA experiments were conducted as previously described (Dupuy et al., 2013; Faubert et al., 2014). Cells ($1–2 \times 10^6$ cells/6 cm dish) were grown for 24 hr, followed by incubation for 15–30 min in glucose or glutamine-free medium containing 10% dialyzed FBS (Wisent) and uniformly labeled U-[^{13}C]-glucose or U-[^{13}C]-glutamine (Cambridge Isotope Laboratories) (Faubert et al., 2013). All labeling experiments were performed in duplicate and repeated three times; the graphs correspond to one representative experiment.

Microarray Analysis

RNA was extracted from 4T1 parental and individual in vivo selected metastatic subpopulations; purified total RNA was subjected to amplification and hybridized to 44K whole-mouse genome microarray gene expression chips (Agilent Technologies, Mississauga, ON, Canada) as described previously (Tabariès et al., 2015). The microarray data can be accessed through the GEO repository (ID GSE62598).

HIF Reporter Assay

Breast cancer cells were cotransfected with a HIF luciferase reporter (pGL2-TK-HRE, 0.5 μg) (Rapisarda et al., 2002) and a Renilla luciferase expression vector (0.25 μg). Luciferase activity in transfected cells was determined 48 hr later by Dual-Glo Luciferase Assay (Promega, Madison, WI, USA) and normalized to Renilla luciferase activity. HIF-dependent luciferase activity

was measured under basal conditions, or following 24 hr incubation in 1% oxygen. The data are expressed as the fold change in HIF reporter activity relative to 4T1 cells and correspond to an average of three experiments performed in duplicate.

Immunoblotting and qPCR

Immunoblots were performed as previously described (Tabariès et al., 2011). RNA extraction, cDNA synthesis, and qPCR were performed as previously described (Dupuy et al., 2013). Real-time qPCR was performed using an Applied Biosystems 7500 instrument (Applied Biosystems) using the primers listed in Table S4. Transcript expression was determined relative to Rpl13 mRNA levels and expressed as the fold change compared to control 4T1 cells. The data represent the average of three independent experiments from three biological replicates per experiment.

In Vivo Tumor Growth and Metastatic Seeding Assays

1×10^4 cells were injected into the mammary fat pads of Balb/c mice to assess primary tumor cell growth as previously described (Tabariès et al., 2011). For experimental metastasis assays, 1×10^5 cells were injected into the spleens or the tail vein of female Balb/c mice as previously described (Tabariès et al., 2011) to assess metastatic potential to the liver and lung, respectively. For short-term in vivo seeding assay, CFSE-labeled (Invitrogen) cells (1×10^5) were subjected to splenic injection as previously described (Tabariès et al., 2012). After 2, 26, and 50 hr postinjection, seven to ten mice per cohort were sacrificed, and livers were collected and whole-mounted for imaging. The number of extravasated CFSE-labeled breast cancer cells per field was assessed using an inverted microscope (Zeiss Axiozoom.V16), and seven fields were quantified per animal. The mice were housed in facilities managed by the McGill University Animal Resources Centre, and all animal experiments were conducted under a McGill University-approved Animal Use Protocol in accordance with guidelines established by the Canadian Council on Animal Care.

Human Clinical Samples, Immunohistochemistry, and Scoring

Tissue microarrays (TMAs) were designed and constructed as described previously (Hsu et al., 2002; Makretsov et al., 2003). Immunohistochemical staining for PDK-1 was performed on paraffin-embedded sections using an anti-PDHK-1 antibody (1:50 dilution, C47H1 #3820, Cell Signaling Technology, Danvers, MA).

Statistical Analyses

Data are presented as mean ± SD for technical replicates, or mean ± SEM for biological replicates, and analyzed using unpaired Student's t test (VassarStats software). Statistical significance is indicated in all figures by the following annotations: $^*p < 0.05$; $^{**}p < 0.01$; $^{***}p < 0.001$.

SUPPLEMENTAL INFORMATION

Supplemental Information includes six figures, four tables, and Supplemental Experimental Procedures and can be found with this article at http://dx.doi.org/10.1016/j.cmet.2015.08.007.

AUTHOR CONTRIBUTIONS

Experimental design was conducted by F.D., R.G.J., and P.M.S., and the majority of experiments executed by F.D. Data interpretation was performed by F.D., E.E.V., J.S.-P., R.G.J., and P.M.S. Microarray analysis was performed by S.T. Mammary fat pad and splenic injections were done by F.D. and S.T. Tail vein injections were performed by M.G.A. Respiration assays were performed by S.A. and F.D. Mitochondrial ROS staining was done by J.B. and F.D. Authors E.A., M.C., A.A.-M., and M.B. provided primary breast tumor samples and matched metastases (liver and skin) used in this study. Immunohistochemistry staining of PDK1 was performed by Z.D. The TMA was scored by D.G., and the analysis of PDK1 expression with breast cancer specific survival was performed by S.L. PDK1 staining of the primary breast tumors and matched liver metastases was scored by A.O. The manuscript was written by F.D. and edited by F.D., R.G.J., and P.M.S.

ACKNOWLEDGMENTS

We acknowledge technical assistance from the McGill/GCRC Histology (Jo-Ann Bader) and Metabolomics (Daina Avizonis and Luc Choiniere) facilities. We thank Dr. Torsten Nielsen and Christine Chow for analysis of PDK1 staining of breast tumor TMAs. We also thank the FRQS Réseau de Recherche en Santé, axe Cancer du Sein, for support of the metastatic breast tumor biobank; Drs. Arnim Pause and Sidong Huang for reagents; and Dr. Véronique Ouellet for bioinformatics support. We thank Dr. Ursini-Siegel and members of the Siegel and Jones laboratories for their scientific input and critical reading of the manuscript. The GCRC Metabolomics Core Facility is supported by grants from the Canadian Foundation for Innovation (CFI) and Canadian Institutes of Health Research (CIHR)/Terry Fox Research Institute (TFRI). We acknowledge salary support from the McGill Integrated Cancer Research Training Program (to F.D. and S.A.), McGill Department of Medicine (S.T.), CIHR (to R.G.J.), and FRQS (to J.B., J.S.-P., and P.M.S.). This research has been supported by grants from the CIHR (MOP-93799 to R.G.J.; MOP-136907 to P.M.S.) and TFRI (TFRI-239585 to R.G.J. and P.M.S.). This work is dedicated to the memory of Rosalind Goodman.

Received: February 27, 2015
Revised: June 27, 2015
Accepted: August 8, 2015
Published: September 10, 2015

REFERENCES

Ahn, C.S., and Metallo, C.M. (2015). Mitochondria as biosynthetic factories for cancer proliferation. Cancer Metab. *3*, 1.

Aslakson, C.J., and Miller, F.R. (1992). Selective events in the metastatic process defined by analysis of the sequential dissemination of subpopulations of a mouse mammary tumor. Cancer Res. *52*, 1399–1405.

Bonnet, S., Archer, S.L., Allalunis-Turner, J., Haromy, A., Beaulieu, C., Thompson, R., Lee, C.T., Lopaschuk, G.D., Puttagunta, L., Bonnet, S., et al. (2007). A mitochondria-K+ channel axis is suppressed in cancer and its normalization promotes apoptosis and inhibits cancer growth. Cancer Cell *11*, 37–51.

Chiavarina, B., Whitaker-Menezes, D., Martinez-Outschoorn, U.E., Witkiewicz, A.K., Birbe, R., Howell, A., Pestell, R.G., Smith, J., Daniel, R., Sotgia, F., and Lisanti, M.P. (2011). Pyruvate kinase expression (PKM1 and PKM2) in cancer-associated fibroblasts drives stromal nutrient production and tumor growth. Cancer Biol. Ther. *12*, 1101–1113.

DeBerardinis, R.J., Mancuso, A., Daikhin, E., Nissim, I., Yudkoff, M., Wehrli, S., and Thompson, C.B. (2007). Beyond aerobic glycolysis: transformed cells can engage in glutamine metabolism that exceeds the requirement for protein and nucleotide synthesis. Proc. Natl. Acad. Sci. USA *104*, 19345–19350.

Dickins, R.A., Hemann, M.T., Zilfou, J.T., Simpson, D.R., Ibarra, I., Hannon, G.J., and Lowe, S.W. (2005). Probing tumor phenotypes using stable and regulated synthetic microRNA precursors. Nat. Genet. *37*, 1289–1295.

Dupuy, F., Griss, T., Blagih, J., Bridon, G., Avizonis, D., Ling, C., Dong, Z., Siwak, D.R., Annis, M.G., Mills, G.B., et al. (2013). LKB1 is a central regulator of tumor initiation and pro-growth metabolism in ErbB2-mediated breast cancer. Cancer Metab. *1*, 18.

Faubert, B., Boily, G., Izreig, S., Griss, T., Samborska, B., Dong, Z., Dupuy, F., Chambers, C., Fuerth, B.J., Viollet, B., et al. (2013). AMPK is a negative regulator of the Warburg effect and suppresses tumor growth in vivo. Cell Metab. *17*, 113–124.

Faubert, B., Vincent, E.E., Griss, T., Samborska, B., Izreig, S., Svensson, R.U., Mamer, O.A., Avizonis, D., Shackelford, D.B., Shaw, R.J., and Jones, R.G. (2014). Loss of the tumor suppressor LKB1 promotes metabolic reprogramming of cancer cells via HIF-1α. Proc. Natl. Acad. Sci. USA *111*, 2554–2559.

Hanahan, D., and Weinberg, R.A. (2011). Hallmarks of cancer: the next generation. Cell *144*, 646–674.

Hassoun, E.A., and Ray, S. (2003). The induction of oxidative stress and cellular death by the drinking water disinfection by-products, dichloroacetate and trichloroacetate in J774.A1 cells. Comparative biochemistry and

physiology. Toxicology & pharmacology. Comp. Biochem. Physiol. C Toxicol. Pharmacol. *135*, 119–128.

Hensley, C.T., Wasti, A.T., and DeBerardinis, R.J. (2013). Glutamine and cancer: cell biology, physiology, and clinical opportunities. J. Clin. Invest. *123*, 3678–3684.

Hsu, F.D., Nielsen, T.O., Alkushi, A., Dupuis, B., Huntsman, D., Liu, C.L., van de Rijn, M., and Gilks, C.B. (2002). Tissue microarrays are an effective quality assurance tool for diagnostic immunohistochemistry. Mod. Pathol. *15*, 1374–1380.

Huang, S., Hölzel, M., Knijnenburg, T., Schlicker, A., Roepman, P., McDermott, U., Garnett, M., Grernrum, W., Sun, C., Prahallad, A., et al. (2012). MED12 controls the response to multiple cancer drugs through regulation of TGF-β receptor signaling. Cell *151*, 937–950.

Keith, B., Johnson, R.S., and Simon, M.C. (2012). HIF1α and HIF2α: sibling rivalry in hypoxic tumour growth and progression. Nat. Rev. Cancer *12*, 9–22.

Kim, J.W., Tchernyshyov, I., Semenza, G.L., and Dang, C.V. (2006). HIF-1-mediated expression of pyruvate dehydrogenase kinase: a metabolic switch required for cellular adaptation to hypoxia. Cell Metab. *3*, 177–185.

Kumar, A., Kant, S., and Singh, S.M. (2012). Novel molecular mechanisms of antitumor action of dichloroacetate against T cell lymphoma: Implication of altered glucose metabolism, pH homeostasis and cell survival regulation. Chem. Biol. Interact. *199*, 29–37.

LeBleu, V.S., O'Connell, J.T., Gonzalez Herrera, K.N., Wikman, H., Pantel, K., Haigis, M.C., de Carvalho, F.M., Damascena, A., Domingos Chinen, L.T., Rocha, R.M., et al. (2014). PGC-1alpha mediates mitochondrial biogenesis and oxidative phosphorylation in cancer cells to promote metastasis. Nat. Cell Biol. *16*, 992–1003, 1001–1015.

Lu, X., Bennet, B., Mu, E., Rabinowitz, J., and Kang, Y. (2010). Metabolomic changes accompanying transformation and acquisition of metastatic potential in a syngeneic mouse mammary tumor model. J. Biol. Chem. *285*, 9317–9321.

Makretsov, N., Gilks, C.B., Coldman, A.J., Hayes, M., and Huntsman, D. (2003). Tissue microarray analysis of neuroendocrine differentiation and its prognostic significance in breast cancer. Hum. Pathol. *34*, 1001–1008.

Martinez-Outschoorn, U.E., Lisanti, M.P., and Sotgia, F. (2014). Catabolic cancer-associated fibroblasts transfer energy and biomass to anabolic cancer cells, fueling tumor growth. Semin. Cancer Biol. *25*, 47–60.

Metallo, C.M., Gameiro, P.A., Bell, E.L., Mattaini, K.R., Yang, J., Hiller, K., Jewell, C.M., Johnson, Z.R., Irvine, D.J., Guarente, L., et al. (2012). Reductive glutamine metabolism by IDH1 mediates lipogenesis under hypoxia. Nature *481*, 380–384.

Nieman, K.M., Kenny, H.A., Penicka, C.V., Ladanyi, A., Buell-Gutbrod, R., Zillhardt, M.R., Romero, I.L., Carey, M.S., Mills, G.B., Hotamisligil, G.S., et al. (2011). Adipocytes promote ovarian cancer metastasis and provide energy for rapid tumor growth. Nat. Med. *17*, 1498–1503.

Papandreou, I., Cairns, R.A., Fontana, L., Lim, A.L., and Denko, N.C. (2006). HIF-1 mediates adaptation to hypoxia by actively downregulating mitochondrial oxygen consumption. Cell Metab. *3*, 187–197.

Porporato, P.E., Payen, V.L., Pérez-Escuredo, J., De Saedeleer, C.J., Danhier, P., Copetti, T., Dhup, S., Tardy, M., Vazeille, T., Bouzin, C., et al. (2014). A mitochondrial switch promotes tumor metastasis. Cell Rep. *8*, 754–766.

Rapisarda, A., Uranchimeg, B., Scudiero, D.A., Selby, M., Sausville, E.A., Shoemaker, R.H., and Melillo, G. (2002). Identification of small molecule inhibitors of hypoxia-inducible factor 1 transcriptional activation pathway. Cancer Res. *62*, 4316–4324.

Rose, A.A., Pepin, F., Russo, C., Abou Khalil, J.E., Hallett, M., and Siegel, P.M. (2007). Osteoactivin promotes breast cancer metastasis to bone. Mol. Cancer Res. *5*, 1001–1014.

Rose, A.A., Annis, M.G., Dong, Z., Pepin, F., Hallett, M., Park, M., and Siegel, P.M. (2010). ADAM10 releases a soluble form of the GPNMB/Osteoactivin extracellular domain with angiogenic properties. PLoS ONE *5*, e12093.

Semenza, G.L. (2013). HIF-1 mediates metabolic responses to intratumoral hypoxia and oncogenic mutations. J. Clin. Invest. *123*, 3664–3671.

Sun, R.C., and Denko, N.C. (2014). Hypoxic regulation of glutamine metabolism through HIF1 and SIAH2 supports lipid synthesis that is necessary for tumor growth. Cell Metab. *19*, 285–292.

Sutendra, G., Dromparis, P., Kinnaird, A., Stenson, T.H., Haromy, A., Parker, J.M., McMurtry, M.S., and Michelakis, E.D. (2013). Mitochondrial activation by inhibition of PDKII suppresses HIF1a signaling and angiogenesis in cancer. Oncogene *32*, 1638–1650.

Tabariès, S., Dong, Z., Annis, M.G., Omeroglu, A., Pepin, F., Ouellet, V., Russo, C., Hassanain, M., Metrakos, P., Diaz, Z., et al. (2011). Claudin-2 is selectively enriched in and promotes the formation of breast cancer liver metastases through engagement of integrin complexes. Oncogene *30*, 1318–1328.

Tabariès, S., Dupuy, F., Dong, Z., Monast, A., Annis, M.G., Spicer, J., Ferri, L.E., Omeroglu, A., Basik, M., Amir, E., et al. (2012). Claudin-2 promotes breast cancer liver metastasis by facilitating tumor cell interactions with hepatocytes. Mol. Cell. Biol. *32*, 2979–2991.

Tabariès, S., Ouellet, V., Hsu, B.E., Annis, M.G., Rose, A.A., Meunier, L., Carmona, E., Tam, C.E., Mes-Masson, A.M., and Siegel, P.M. (2015). Granulocytic immune infiltrates are essential for the efficient formation of breast cancer liver metastases. Breast Cancer Res. *17*, 45.

Vander Heiden, M.G., Cantley, L.C., and Thompson, C.B. (2009). Understanding the Warburg effect: the metabolic requirements of cell proliferation. Science *324*, 1029–1033.

Warburg, O. (1956). On the origin of cancer cells. Science *123*, 309–314.

Ward, P.S., and Thompson, C.B. (2012). Metabolic reprogramming: a cancer hallmark even warburg did not anticipate. Cancer Cell *21*, 297–308.

Wise, D.R., Ward, P.S., Shay, J.E., Cross, J.R., Gruber, J.J., Sachdeva, U.M., Platt, J.M., DeMatteo, R.G., Simon, M.C., and Thompson, C.B. (2011). Hypoxia promotes isocitrate dehydrogenase-dependent carboxylation of α-ketoglutarate to citrate to support cell growth and viability. Proc. Natl. Acad. Sci. USA *108*, 19611–19616.

Yan, M., Gingras, M.C., Dunlop, E.A., Nouët, Y., Dupuy, F., Jalali, Z., Possik, E., Coull, B.J., Kharitidi, D., Dydensborg, A.B., et al. (2014). The tumor suppressor folliculin regulates AMPK-dependent metabolic transformation. J. Clin. Invest. *124*, 2640–2650.

Yuneva, M.O., Fan, T.W., Allen, T.D., Higashi, R.M., Ferraris, D.V., Tsukamoto, T., Matés, J.M., Alonso, F.J., Wang, C., Seo, Y., et al. (2012). The metabolic profile of tumors depends on both the responsible genetic lesion and tissue type. Cell Metab. *15*, 157–170.